GEOPHYSICS, VOL. 80, NO. 6 (NOVEMBER-DECEMBER 2015); P. KS69–KS80, 18 FIGS.
10.1190/GEO2014-0423.1

Microseismic and seismic denoising via ensemble empirical mode decomposition and adaptive thresholding

Jiajun Han[1] and Mirko van der Baan[2]

ABSTRACT

Random and coherent noise exists in microseismic and seismic data, and suppressing noise is a crucial step in seismic processing. We have developed a novel seismic denoising method, based on ensemble empirical mode decomposition (EEMD) combined with adaptive thresholding. A signal was decomposed into individual components called *intrinsic mode functions* (IMFs). Each decomposed signal was then compared with those IMFs resulting from a white-noise realization to determine if the original signal contained structural features or white noise only. A thresholding scheme then removed all nonstructured portions. Our scheme is very flexible, and it is applicable in a variety of domains or in a diverse set of data. For instance, it can serve as an alternative for random noise removal by band-pass filtering in the time domain or spatial prediction filtering in the frequency-offset domain to enhance the lateral coherence of seismic sections. We have determined its potential for microseismic and reflection seismic denoising by comparing its performance on synthetic and field data using a variety of methods including band-pass filtering, basis pursuit denoising, frequency-offset deconvolution, and frequency-offset empirical mode decomposition.

INTRODUCTION

Empirical mode decomposition (EMD) developed by Huang et al. (1998) is a powerful signal analysis technique to split nonstationary and nonlinear signal systems, such as seismic data. Through the extraction of intrinsic mode functions (IMFs), EMD captures the nonstationary features of the input signal. EMD has several interesting properties that make it an attractive tool for signal analysis: It results in complete signal decomposition; i.e., the original signal is reconstructed by summing all IMFs. No loss of information is incurred. The EMD is a quasi-orthogonal decomposition in that the crosscorrelation coefficients between the different IMFs are always close to zero. This minimizes energy leakage between the IMFs (Bekara and Van der Baan, 2009). Based on these promising characteristics, Magrin-Chagnolleau and Baraniuk (1999) and Han and Van der Baan (2011) apply EMD for robust seismic attribute analysis, Battista et al. (2007) exploit EMD to remove cable strum noise, Bekara and Van der Baan (2009) propose the frequency-offset (*f-x*) EMD technique to suppress the seismic random and coherent noise, Xue et al. (2014) use EMD with the Teager-Kaiser method for hydrocarbon detection, and recently Chen and Ma (2014) combine *f-x* EMD and autoregressive (AR) model to deal with complex subsurface structures.

Even though EMD offers several promising properties, some features encumber its direct applications, namely, mode mixing and splitting, aliasing, and end-point artifacts (Mandic et al., 2013; Tary et al., 2014). Two variants were recently introduced to overcome some of the negative features associated with EMD, namely *ensemble EMD* (EEMD) (Wu and Huang, 2009) and *complete ensemble EMD* (CEEMD) (Torres et al., 2011). Tong et al. (2012) compare the superiority of EEMD over EMD on seismic time-frequency analysis, Song et al. (2012) extend the EEMD to seismic oceanography for analyzing ocean internal waves. Recently, Han and Van der Baan (2013) successfully combine CEEMD with instantaneous spectra for seismic spectral decomposition.

Denoising via EMD started from examining the properties of IMFs resulting from white Gaussian noise (Flandrin et al., 2004b). The first attempt is detrending and denoising electrocardiogram signals by partial reconstructions with the selected IMFs (Flandrin et al., 2004a). However, this approach has the disadvantage that even if the appropriate IMFs are selected, they still may be noise contaminated. Boudraa and Cexus (2006) improve the denoising scheme by using adaptive thresholding and a Savitzky-Golay

Manuscript received by the Editor 7 September 2014; revised manuscript received 25 May 2015; published online 18 August 2015.
[1]Formerly University of Alberta, Department of Physics, Edmonton, Canada; presently Hampson-Russell Limited Partnership, A CGG Company, Calgary, Alberta, Canada. E-mail: jiajun.han@cgg.com.
[2]University of Alberta, Department of Physics, Edmonton, Alberta, Canada. E-mail: mirko.vanderbaan@ualberta.ca.

filter for each IMF, respectively. Inspired by translation-invariant wavelet thresholding, Kopsinis and McLaughlin (2009) propose an iterative EMD denoising method to enhance the original method. Recently, hybrid EMD denoising methods, based on higher order statistics and the curvelet transform, have also been proposed (Tsolis and Xenos, 2011; Dong et al., 2013).

In seismic processing, the *f-x* domain plays a significant role because linear or quasilinear events in the time-offset (*t-x*) domain manifest themselves as a superposition of harmonics in the *f-x* domain. Canales (1984) first proposes prediction error filtering, based on an AR model in the *f-x* domain to attenuate random noise, which is widely known as *f-x* deconvolution. However, the AR model assumes that the error is an innovation sequence rather than additive noise. Soubaras (1994) introduces *f-x* projection filtering to circumvent this problem by using the AR-moving average (ARMA) model instead of the AR model. Sacchi and Kuehl (2001) further discuss the ARMA formulation in the *f-x* domain and discover that the ARMA coefficients can be computed by solving an eigenvalue problem. Integration of EMD into the *f-x* domain is first investigated by Bekara and Van der Baan (2009). They find that eliminating the first IMF component in each frequency slice corresponds to an autoadaptive wavenumber filter. This process reduces the random and steeply dipping coherent noise in the seismic data. Instead of directly deleting the first IMF in the *f-x* domain, Chen and Ma (2014) apply the AR model on the first IMF to enhance the original *f-x* EMD performance.

In this paper, we first propose a novel method for suppressing random noise based on the EEMD principle. Next, we test the proposed EEMD thresholding on low- and high-signal-to-noise-ratio (S/N) synthetic and microseismic examples. Finally, we extend the proposed method into the *f-x* domain to suppress random and coherent noise in seismic data.

THEORY

Empirical mode decomposition and ensemble empirical mode decomposition

EMD is a fully data-driven separation of a data series into fast and slow oscillation components, and these decomposed components are called IMFs. The IMFs are computed recursively, starting with the most oscillatory one. The decomposition method uses the envelopes defined by the local maxima and the local minimum of the data series. Once the maxima of the original signal are identified, cubic splines are used to interpolate all the local maxima and construct the upper envelope. The same procedure is used for the local minimum to obtain the lower envelope. Next, one calculates the average of the upper and lower envelopes and subtracts it from the initial signal. This interpolation process is continued on the remainder. This sifting process terminates when the mean envelope is reasonably zero everywhere, and the resultant signal is designated as the first IMF. The first IMF is subtracted from the data, and the difference is treated as a new signal on which the same sifting procedure is applied to obtain the next IMF. The decomposition is stopped when the last IMF has a small amplitude or becomes monotonic. The sifting procedure ensures the first IMFs contain the detailed components of the input signal; the last one solely describes the signal trend (Huang et al., 1998; Bekara and Van der Baan, 2009; Han and Van der Baan, 2013).

The IMFs satisfy two conditions: (1) the number of extrema and the number of zero crossings either equal or differ by one and (2) at any point, the mean value of the envelope defined by the local maxima and the envelope defined by the local minimums is zero. These conditions are necessary to make each IMF after decomposition a symmetric, narrowband waveform, which ensures that the instantaneous frequency is smooth and positive.

However, EMD suffers from several drawbacks (Mandic et al., 2013). The most severe one is mode mixing, which is defined as a single IMF consisting of signals of widely disparate scales or a signal of a similar scale residing in different IMF components (Huang and Wu, 2008). The EEMD, briefly speaking, is EMD combined with noise stabilization. Using the injection of controlled zero mean, Gaussian white noise, EEMD effectively reduces mode mixing (Wu and Huang, 2009; Mandic et al., 2013). Adding white Gaussian noise helps perturb the signal and enables the EMD algorithm to visit all possible solutions in the finite neighborhood of the final answer, and it also takes advantage of the zero mean of the noise to cancel aliasing (Wu and Huang, 2009). The implementation procedure for EEMD is simple and is as follows:

1) Add a fixed percentage of Gaussian white noise onto the target signal.
2) Decompose the resulting signal into IMFs.
3) Repeat steps (1) and (2) several times, using different noise realizations.
4) Obtain the ensemble averages of the corresponding individual IMFs.

The EEMD is a noise injection technique, and the added Gaussian white noises are zero mean with a constant flat-frequency spectrum. Their contribution thus cancels out and does not introduce signal components that are not already present in the original data. The ensemble-averaged IMFs therefore maintain their natural dyadic properties and effectively reduce the chance of mode mixing (Han and Van der Baan, 2013).

Ensemble empirical mode decomposition thresholding

The first attempt at using EMD as a denoising tool emerged from the need to know whether a specific IMF contains useful information or primarily noise. Thus, Flandrin et al. (2004b) and Wu and Huang (2004) nearly simultaneously investigate the EMD feature for Gaussian noise, and they conclude that EMD acts essentially as a dyadic filter bank resembling those involved in wavelet decomposition. Therefore, the energy of each IMF from white Gaussian noise follows an exponential relationship, and Kopsinis and McLaughlin (2009) refine this relationship as

$$E_k^2 = E_1^2/0.719 \times 2.01^{-k}, \tag{1}$$

where E_k^2 is the energy of the kth IMF, and the parameters 0.719 and 2.01 are empirically calculated from numerical tests. Because the IMFs resemble the wavelet decomposition component, the energy of the first IMF E_1^2 can be estimated using a robust estimator based on the component's median (Donoho and Johnstone, 1994; Herrera et al., 2014):

$$E_1^2 = (\text{median}(|\text{IMF1}(i)|)/0.6755)^2, \quad i = 1, \ldots, n, \tag{2}$$

where n is the length of the input signal. Then, we can set the adaptive threshold T_k in each IMF for suppressing the random noise as

$$T_k = \sigma\sqrt{(2 \times ln(n))} \times E_k, \tag{3}$$

where σ is the main parameter to be set. The combination of equations 2 and 3 is a universal threshold for removing the white Gaussian noise in the wavelet domain (Donoho and Johnstone, 1994; Donoho, 1995).

Followed by the above procedures, the reconstructed signal $\hat{s}$ is expressed as

$$\hat{s} = \sum_{k=m1}^{M-m2} T_k[\mathrm{IMF}_k] + \sum_{k=M-m2+1}^{M} \mathrm{IMF}_k; \tag{4}$$

thresholding is only applied between the $m1 - th$ and $(M - m2)$th IMFs, and the first $(m1 - 1)$th IMFs are removed, where IMF_k is the kth IMF and M is the total number of IMFs of the input signal. If $m2$ is set to 0, we apply the thresholding from the $m1$th IMF to the last IMF. The implemented threshold method is IMF interval thresholding (Kopsinis and McLaughlin, 2009), which is presented in the next section.

Due to the mode mixing of EMD, direct application of the above procedure may not achieve the best effect. Kopsinis and McLaughlin (2009) try to alter the input signal by circle shifting its IMF1 component and adding the circle-shifted IMF1 back to create a different noisy version of the signal. This works if IMF1 only contains noise when the input signal S/N is low, and the circle shifting does not change the embedded useful signal information. Averaging of the denoised outputs of different triggered signals can enhance the final result. However, when the input signal's S/N is high, directly altering IMF1 of the input signal would adversely affect the results.

Considering the different S/N cases, we use the EEMD principle to improve the EMD denoising performance. The procedure of EEMD denoising is as below:

1) Create white Gaussian noise.
2) Calculate the IMF1 of the white Gaussian noise and add it onto the target signal using a predefined S/N.
3) Decompose the resulting signal into IMFs.
4) Apply the EMD denoising principle to the resulting IMFs.
5) Repeat steps (1–4) several times with different noise realizations, and
6) Compute the ensemble denoising average as the final output.

Although not adding the whole white Gaussian noise sequence onto the target signal does not exactly respect the EEMD principle, it shows better results in our synthetic and real data examples rather than a denoising procedure exactly based on EEMD. Due to the dyadic filter feature of EMD, the IMF1 of white Gaussian noise corresponds to the high-frequency noise. It helps to relieve the mode mixing of EMD to some extent and only affects the high-frequency information of the input signal, which can be compensated by a band-pass filter after the proposed EEMD denoising.

Intrinsic mode function interval thresholding

Each IMF is a fundamental element of the input signal. The local extrema and zero crossings are the basic elements for each IMF due to its symmetric feature. Kopsinis and McLaughlin (2008a) propose IMF interval thresholding, which preserves the smooth feature of each IMF. The idea of IMF interval thresholding is maintaining the whole interval between two zero crossings in each IMF, when the absolute value of local extrema in this interval is larger than the threshold. Taking hard thresholding as an example, the expression of direct hard thresholding is

$$\hat{h}(t) = \begin{cases} h(t), & |h(t)| > T \\ 0, & |h(t)| \le T, \end{cases} \tag{5}$$

where $h(t)$ is the input signal, T is the universal threshold, and $\hat{h}(t)$ is the thresholded signal. The interval hard thresholding is expressed as

$$\hat{h}(\mathbf{z}_j) = \begin{cases} h(\mathbf{z}_j), & |h(r_j)| > T \\ 0, & |h(r_j)| \le T, \end{cases} \tag{6}$$

where $h(\mathbf{z}_j)$ indicates the sample interval between adjacent zeros crossings of the input signal, $h(r_j)$ is the local extrema corresponding to this interval, and $\hat{h}(\mathbf{z}_j)$ is the thresholded output. Due to the conditions of each IMF, this guarantees that there is one and only one local extrema $h(r_j)$ in the interval of $h(\mathbf{z}_j)$.

Figure 1 illustrates the difference between the interval and direct hard thresholding. Figure 1a is an IMF from a microseismic event. Direct thresholding (Figure 1c) creates needless discontinuities, and therefore it can have adverse consequences for the continuity of the reconstructed signal. Luckily, these discontinuities can be effectively reduced by IMF interval thresholding (Figure 1b). The new thresholding method retains the smooth features of each IMF. The portion in the red box highlights the advantages on the IMF interval thresholding.

The above example is for hard interval thresholding, and soft interval thresholding is also based on the same idea. For detailed information about soft interval thresholding, refer to Kopsinis and McLaughlin (2008b).

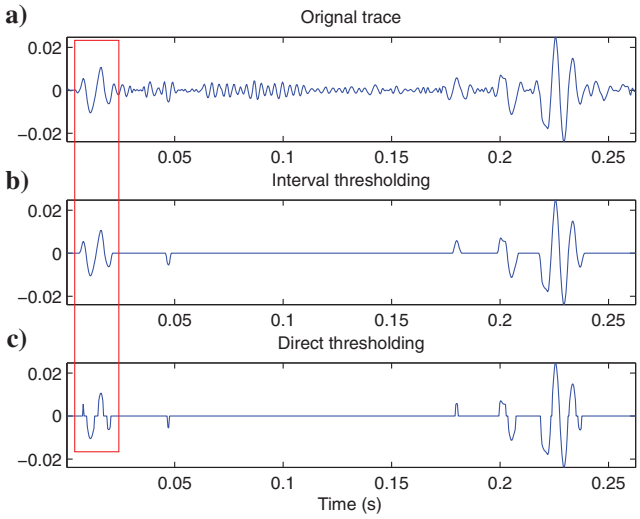

Figure 1. The difference between IMF interval thresholding and direct thresholding. (a) An IMF from a microseismic event. (b) The IMF interval thresholding result. (c) Direct thresholding result. The IMF interval thresholding keeps the smooth features of the IMF, whereas the direct thresholding creates needless discontinuities. The portion in the red box highlights the advantages of IMF interval thresholding.

f-x-domain ensemble empirical mode decomposition thresholding

For the seismic data, one option is applying the proposed EEMD thresholding for each trace for suppressing the random noise. The disadvantage of this approach is not considering the lateral coherence of the seismic reflections. A convenient approach is applying the EEMD thresholding in the *f-x* domain. To process a whole seismic section, *f-x* EEMD thresholding is implemented in a similar way to *f-x* EMD (Bekara and Van der Baan, 2009) and *f-x* deconvolution using the following scheme:

1) Select a time window, and transform the data to the *f-x* domain.
2) For every frequency, separate the real and imaginary parts in the offset sequence.
3) Perform EEMD thresholding on the real and imaginary parts, respectively.
4) Combine to create the filtered complex signal.
5) Transform the data back to the *t-x* domain.
6) Repeat for the next time window.

Bekara and Van der Baan (2009) first propose the *f-x* EMD filter, and they find that IMF1 contains the largest wavenumber components in a constant frequency slice in the *f-x* domain. Therefore, S/N enhancement can be achieved by subtracting IMF1 from the data. In the *f-x* EEMD thresholding implementation, the parameters $m1$ and $m2$ control the threshold range of the IMF order, and parameter σ is related to the noise level. The *f-x* EMD filter is a special case of *f-x* EEMD thresholding with parameters as $\sigma = 0$, $m1 = 2$, and $m2 = 0$. Unlike the *f-x* deconvolution, which uses a fixed filter length for all frequencies, EMD adaptively matches its decomposition to the smoothness of the data. Directly eliminating the IMF1 of a signal means removing its most oscillatory element, and the residual receives a smoother feature. However, only subtracting IMF1 in each constant frequency slice seems to be not enough or too harsh for some seismic data (Chen and Ma, 2014); *f-x* EEMD thresholding thus improves its performance.

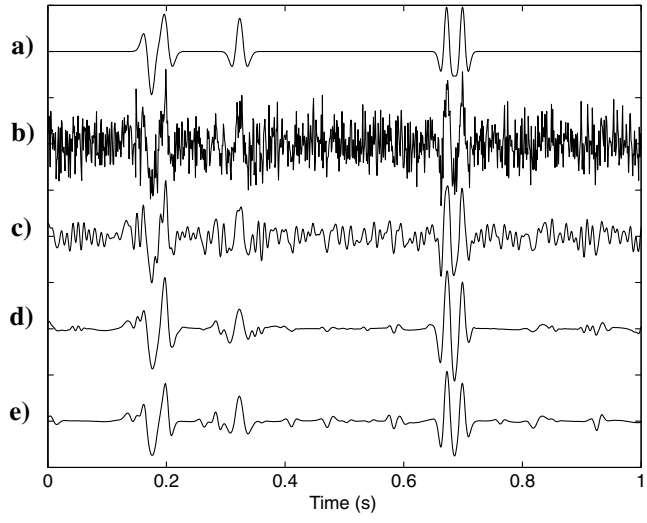

Figure 2. Low-S/N synthetic example. (a) Noise-free trace, (b) noisy trace with S/N = 1, (c) trace after band-pass filtering, (d) trace after EEMD thresholding, and (e) trace after basis pursuit. EEMD thresholding and the basis pursuit suppress more random noise than does band-pass filtering.

EXAMPLES

Synthetic example

Figure 2a shows one trace comprised of several events with 30- and 40-Hz Ricker wavelets. Figure 2b is the noise-contaminated version with an S/N equal to 1. This is a low-S/N case to test our proposed method. Because the proposed method is a single-trace technique, we first compare with an appropriately set band-pass filter (Figure 2c). Because the random noise pollutes the whole frequency domain, a band-pass filter is not an effective method here. Our proposed method with $\sigma = 0.35$, $m1 = 3$, and $m2 = 0$ (Figure 2d) suppresses most of the random noise and better enhances the events, and hence, it drastically improves the S/N of the test data. Note that the same band-pass filter as Figure 2c is applied after the proposed denoising method. Another technique we compare here is the basis pursuit approach (Chen et al., 2001), which has been shown to be an effective tool for suppressing random noise in microseismic and seismic processing (Vera Rodriguez et al., 2012; Han et al., 2014). Basis pursuit with regularization parameter 0.1 (Figure 2e) eliminates most of the random noise. Because the S/N of each trace equals 1, the random noise affects the waveforms severely. Compared with band-pass filtering, the EEMD denoising and basis pursuit techniques effectively eliminate the random noise and protect the useful waveform to the maximum extent.

Figures 3–5 illustrate the principle of EEMD thresholding. The solid line (Figure 3) is the theoretical IMF energy of white Gaussian noise based on equation 3 when $\sigma = 1$, and the dashed line represents the IMF energy of the noisy trace (Figure 2b). The slope of first two IMFs' energy matches the theoretical line the most, which indicates that they are the most similar to the noise characteristic. On the other hand, the other IMFs contain less noise because their energy distribution deviates from the theoretical line. Figure 4 shows the nine IMFs of the noisy trace using EEMD. The first two IMFs contain the highest frequency information, and the least signal information can be found. This agrees with Figure 3. The parameters $m1 = 3$ and $m2 = 0$ indicate that the thresholding is only applied from IMF3 to the last IMF, and it sets the reconstructed

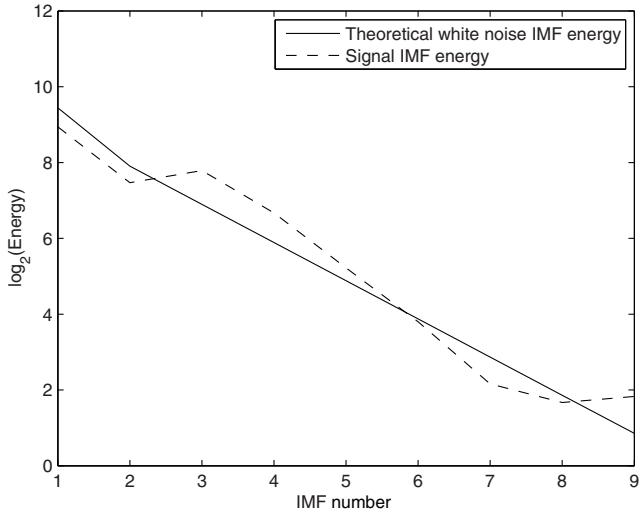

Figure 3. IMF energy distribution of the noisy trace (Figure 2b) and the theoretical IMF energy distribution of white Gaussian noise based on equation 1.

IMF1 and IMF2 to zero. Figure 5 shows the nine thresholded IMFs. The IMF interval thresholding makes the reconstructed IMFs keep the smooth features, meanwhile getting rid of most of the noise. Note that we apply soft thresholding in this synthetic example.

A high-S/N case to test EEMD thresholding is shown in Figure 6. In this test, the S/N for each trace is 2.5 (Figure 6b). The results from band-pass filtering, EEMD thresholding with $\sigma = 0.3$, $m1 = 2$, and $m2 = 0$, and the basis pursuit with regularization parameter 0.05 are shown in the same sequence as Figure 2. All three methods improve the input noisy data (Figure 6b). Like the low S/N case, the EEMD thresholding (Figure 6d) and basis pursuit (Figure 6e) approaches show clearer outputs than the band-pass filter (Figure 6c) because they reduce random noise from the whole frequency band. Compared with the other two methods, EEMD thresholding (Figure 6d) shows the most proximal result to the noise-free one (Figure 6a).

Microseismic example

In this section, we show two microseismic cases to verify the proposed technique. Figure 7a is 1 of 66 microseismic events from a hydraulic fracturing treatment in Canada. Unlike the synthetic ex-

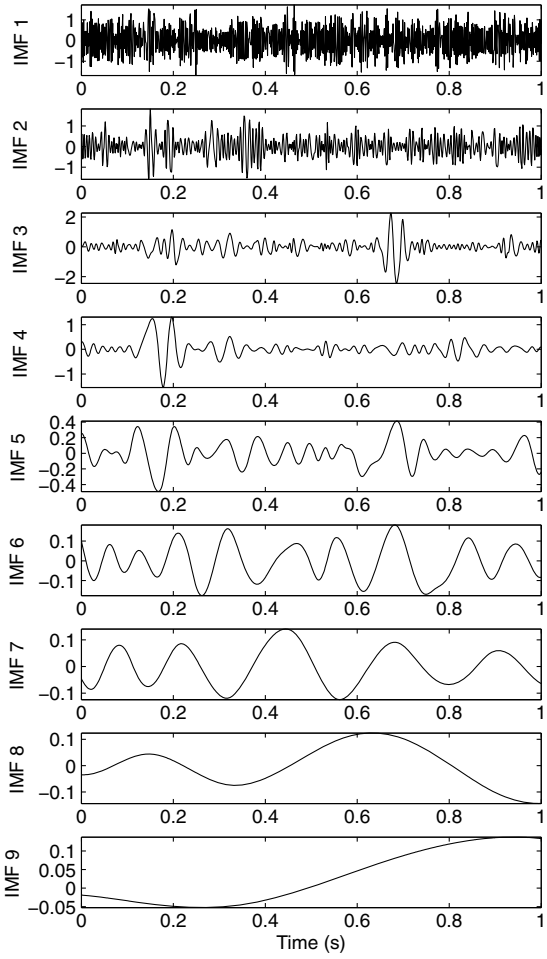

Figure 4. IMFs of the noisy trace: IMF1 and IMF2 contain the highest frequency information, which are out of the interested frequency band.

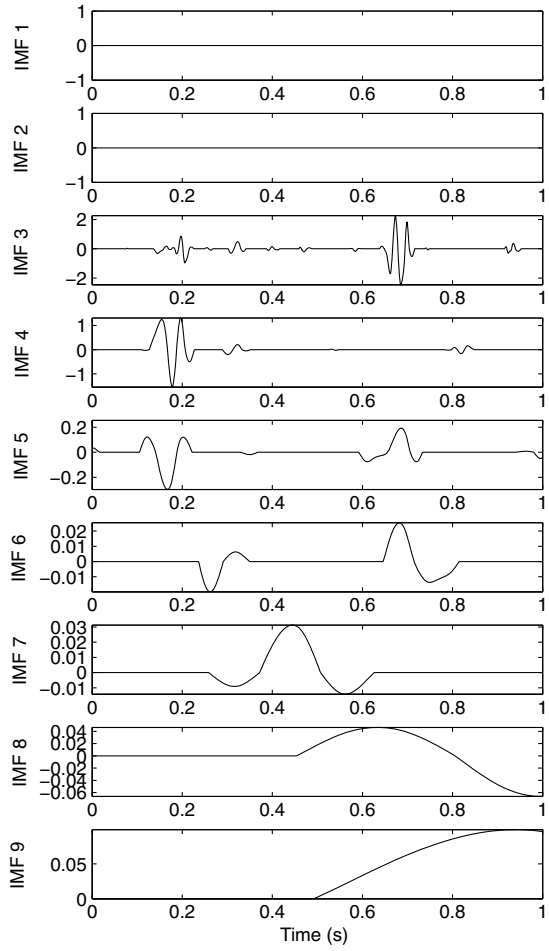

Figure 5. Thresholded IMFs. The reconstructed IMF1 and IMF2 are set as 0. IMF interval thresholding is applied from IMF3 to the last IMF.

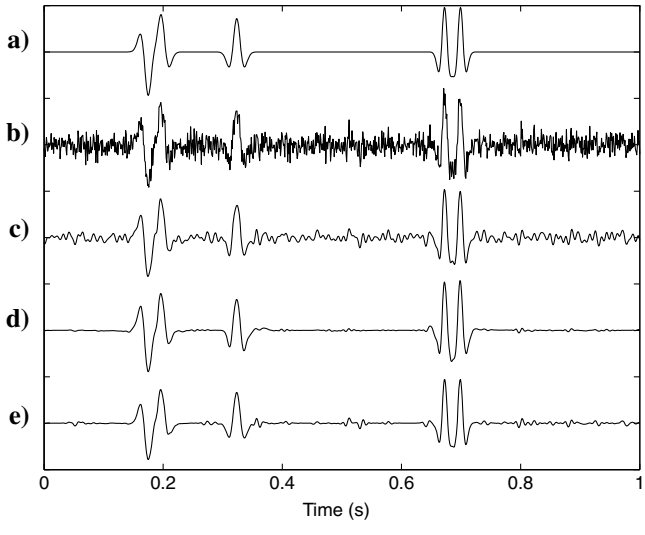

Figure 6. High S/N synthetic example: (a) noise-free trace, (b) noisy trace with S/N = 2.5, (c) trace after band-pass filter, (d) trace after EEMD thresholding, and (e) trace after basis pursuit. EEMD thresholding obtains the smoothest output.

amples, the quality of these microseismic events is much better. The traditional denoising method for microseismic data is band-pass filtering. However, due to the diversity of microseismic data, a fixed frequency range may remove some useful signal. Figure 7b shows the result of a fixed band-pass filter with corner frequencies [1 10 125 180] Hz. Note that this band-pass filter works well for most of the microseismic events in these data, but it removes some of the low-frequency components approximately 0.56 s. Furthermore, there is still some noise before the P-wave arrives.

The proposed EEMD thresholding with $\sigma = 0.6$, $m1 = 2$, and $m2 = 1$, and basis pursuit with regularization parameter 0.005 outputs are shown in Figure 7c and 7d. Like the band-pass filter, they both suppress most of the random noise. Furthermore, these two techniques well preserve the waveform information because they can distinguish the noise and useful information in their own domain. The denoising performance is also confirmed in their spectra (Figure 8). All three methods remove all of the higher frequency noise. The proposed method (Figure 8c) and basis pursuit (Figure 8d) preserve the low-frequency information better than the band-pass filter (Figure 8b). Only EEMD thresholding keeps the components approximately 300 Hz, which probably contains some signal information.

A challenging microseismic test (Castellanos and van der Baan, 2013) is shown in Figure 9, which comes from Saskatchewan in Canada. The raw data (Figure 9a) quality is bad because it not only contains random noise, but also strong electronic noise. High-energy 30-, 60-, and 120-Hz noise components exist in its spectra (Figure 10a). Directly applying the EEMD thresholding and basis pursuit to the raw data would fail because they are only valid for suppressing random noise. A preprocessing step must be accomplished before further processing. Figure 9b is the output after a band-pass filter and notch process of 30 and 60 Hz. The 120-Hz energy is not notched down because it is not visible in the other microseismic events of this experiment.

Even though the preprocessing improves the quality of the raw data, Figure 9b still suffers from severe random noise. The EEMD thresholding (Figure 9c) with $\sigma = 0.25$, $m1 = 1$, and $m2 = 1$ reduces more random noise than the basis pursuit (Figure 9d), and it more effectively (Figure 10c) drops down the 120-Hz energy than

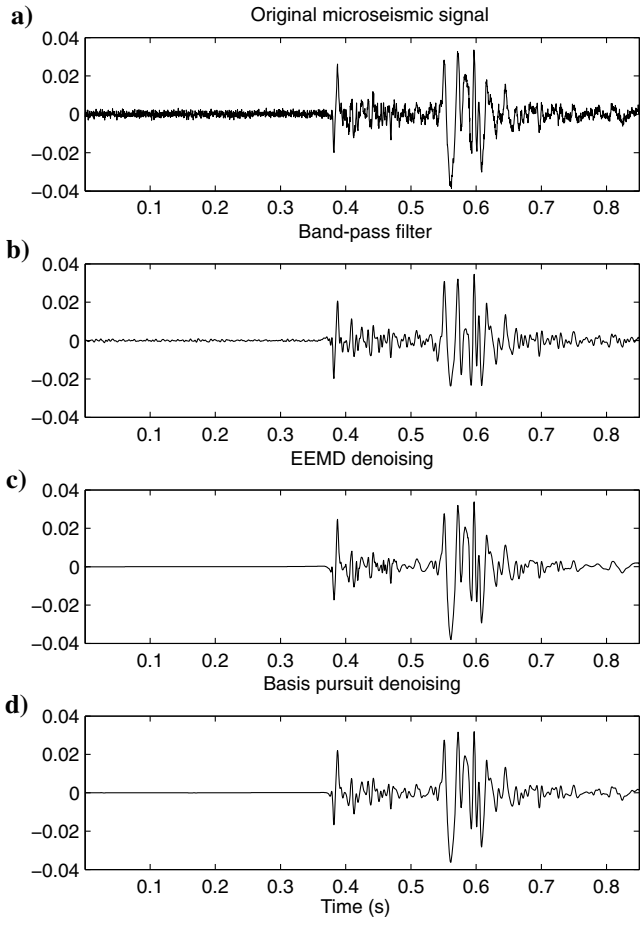

Figure 7. High S/N microseismic event example. (a) Raw microseismic event, (b) band-pass filter output, (c) EEMD thresholding output, and (d) basis pursuit output. The band-pass filter removes some of the low-frequency components at approximately 0.56 s. The proposed method and basis pursuit preserve the waveform better.

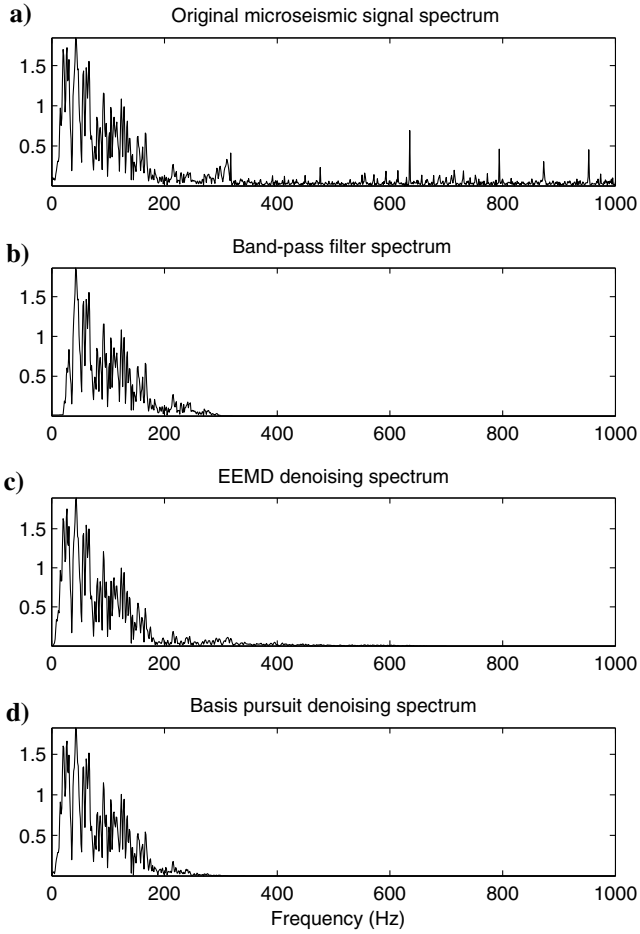

Figure 8. The spectra of Figure 7. (a) Spectra of the original microseismic event, (b) spectra after band-pass filtering, (c) spectra after the proposed method, and (d) spectra after the basis pursuit. Due to the diversity of microseismic data, a fixed frequency range may remove some of the useful signal. EEMD thresholding and the basis pursuit preserve the low-frequency information better than the band-pass filter. Furthermore, EEMD thresholding maintains the components at approximately 300 Hz.

does the basis pursuit method (Figure 10d). Note that the regularization parameter is 35 for basis pursuit implementation. On the other hand, both techniques significantly improve the S/N of the microseismic event, and this is also confirmed in the enlarged part from 0.2 to 0.8 s (Figure 11). The denoising (Figure 11c and 11d) makes the first-arrival pick much easier than on the original microseismic event or after preprocessing. The arrows indicate the first-arrival pick at 0.498 s, which is difficult to detect in Figure 11a and 11b. Denoising of microseismic events can facilitate picking of the first-arrival times and their polarities, which is a crucial step in microseismic processing.

Seismic example

In this section, we verify the performance of *f-x* EEMD thresholding. Figure 12 is a stacked section from Alaska (Geological Survey, 1981). Although the events become continuous after stacking, random, coherent, and background scattered noise still exist, thereby reducing the S/N of the seismic data. We implement EEMD thresholding in the *f-x* domain, mainly because of linear or quasi-linear events in the *t-x* domain manifest as a superposition of harmonics in the *f-x* domain. Therefore, we compare the result with the classic *f-x* deconvolution (Canales, 1984) and *f-x* EMD (Bekara and Van der Baan, 2009).

All three methods are implemented between 0 Hz and 60% of the Nyquist frequency, and frequencies beyond 60% of the Nyquist frequency are damped to zero. The *f-x* EMD only eliminates the IMF1 component in each frequency slice, which makes it a parameter-free technique; *f-x* deconvolution uses the length of the AR operator as 20, prewhitening as 0.1; *f-x* EEMD denoising uses $\sigma = 0.3$, $m1 = 3$, and $m2 = 0$. The outputs of the three methods are shown in Figure 13. All of the techniques enhance the quality of the input data by making the events clearer, especially in the deep part. From the difference sections (Figure 14), neither method loses the reflection information. The *f-x* deconvolution (Figure 14b) and *f-x* EEMD denoising (Figure 14c) seem to eliminate more random noise than

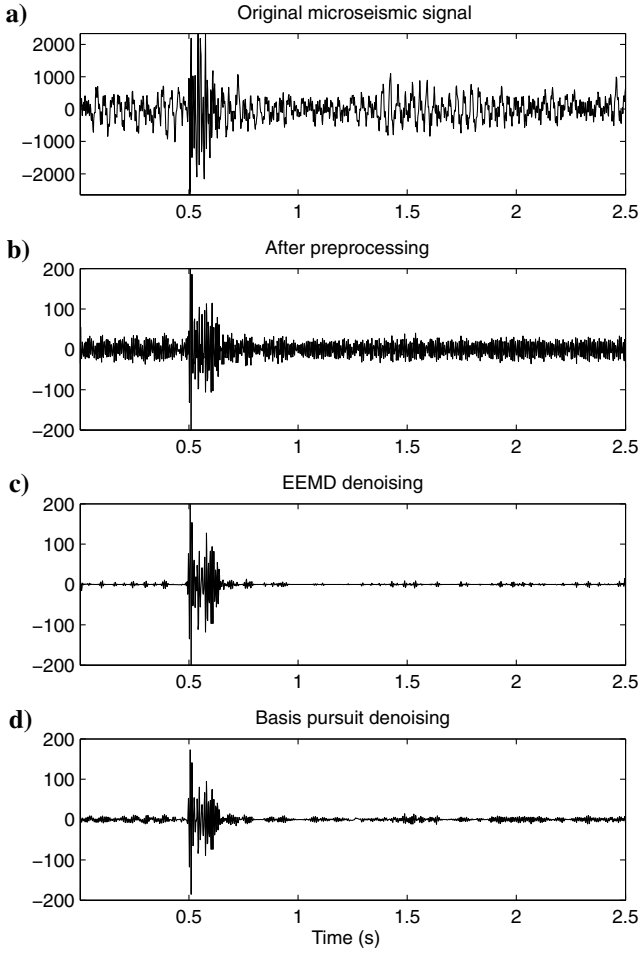

Figure 9. A low-S/N microseismic event example. (a) Raw microseismic event, (b) output after preprocessing, (c) EEMD thresholding output on panel (b), and (d) basis pursuit output on panel (b). The raw microseismic event contains the random noise and electronic noise. The output after preprocessing gets rid of most of the electronic noise. EEMD thresholding and the basis pursuit suppress most of the random noise.

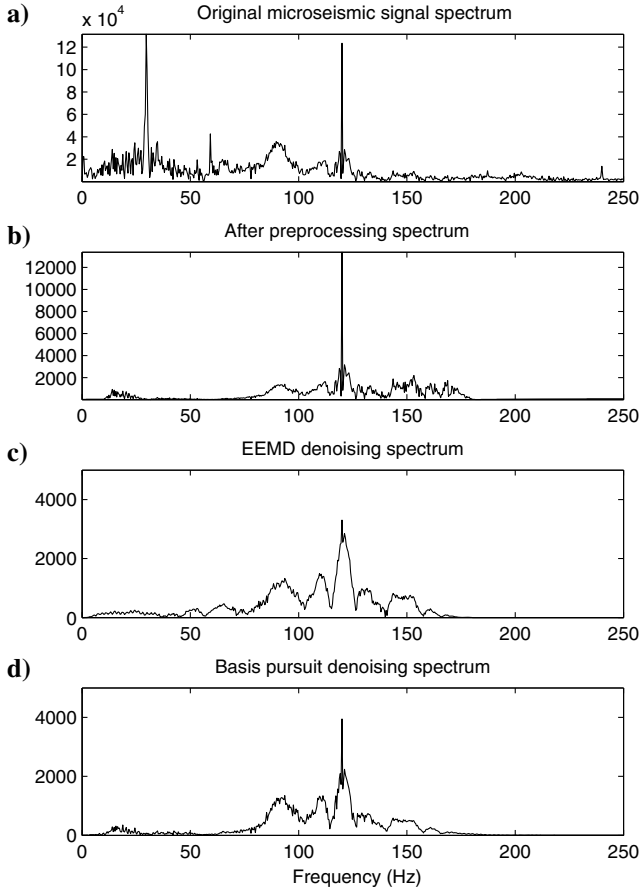

Figure 10. The spectra of Figure 9. (a) Spectra of the raw microseismic event, (b) spectra after preprocessing, (c) spectra after the proposed method in panel (b), and (d) spectra after the basis pursuit in panel (b). There are 30-, 60-, and 120-Hz of electronic noise in the raw microseismic event. The preprocessing reduces the electronic noise at 30 and 60 Hz. The EEMD thresholding and basis pursuit eliminate most of the random noise. The proposed method drops the 120-Hz energy down more effectively than does the basis pursuit approach.

does *f-x* EMD (Figure 17a). The advantage of our proposed method and *f-x* EMD over *f-x* deconvolution is that, except for the random noise, they can eliminate the linear dipping energy as well. Note that all figures are shown on the same amplitude scale.

Figure 15 is the enlarged part of the original data from time 2–3.6 s and CMP number is 1000–3500. It clearly shows that the Alaska data do not contain only random but also coherent noise, such as high-energy linear dipping events. The same enlarged parts of three denoising outputs are shown in Figure 16. The *f-x* EEMD thresholding (Figure 16c) obtains the most satisfactory output, and the events become much clearer. There are still some random and coherent noise in the results of *f-x* EMD (Figure 16a) and *f-x* deconvolution (Figure 16b) in varying degrees. The *f-x* EMD, which eliminates only IMF1 component in each frequency, does not seem to have great impact in the data. The proposed method with parameters $m1 = 3$, $m2 = 0$, and $\sigma = 0.3$ means deleting the first two IMFs and also applying the IMF interval thresholding from IMF3 to the last IMF. This explains why the difference section of the *f-x* EMD (Figure 17a) contains only a portion of noise compared with the one of the proposed methods (Figure 17c). On the other side, because *f-x* deconvolution is only valid for random noise suppression, no dipping noise is shown in its difference profile (Figure 17b).

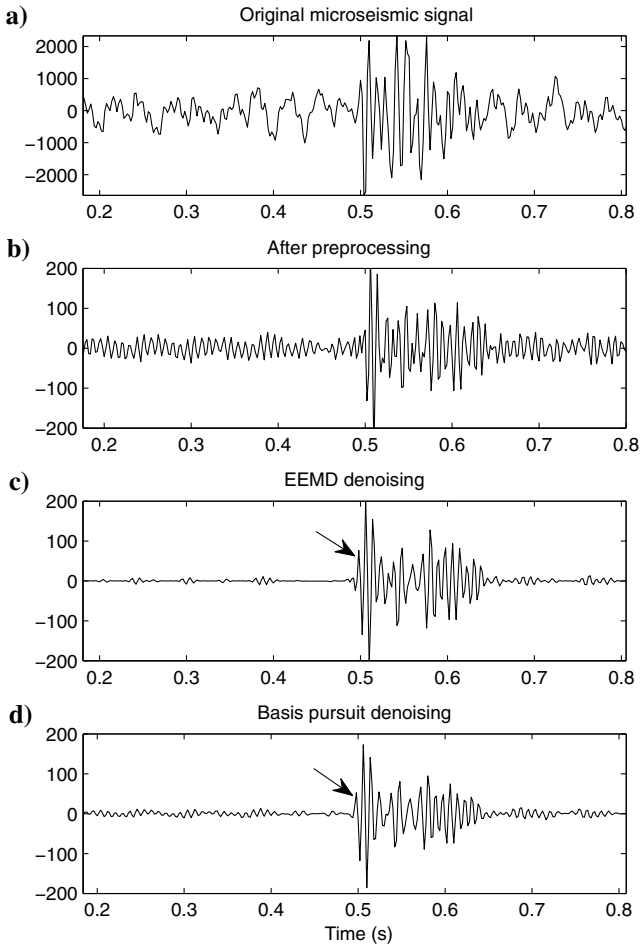

Figure 11. Enlarged part of Figure 9. (a) Original raw microseismic event, (b) output after preprocessing, (c) EEMD thresholding output in panel (b), and (d) basis pursuit output in panel (b). The arrows in panels (c and d) mark the first-arrival times, which are hard to pick on the raw microseismic event (panel [a]) or after preprocessing (panel [b]).

DISCUSSION

Empirical mode decomposition is a fully data-driven technique, and no a priori decomposition basis is chosen such as sines and cosines for the Fourier transform or a mother wavelet for the wavelet transform. The EMD denoising foundation, equation 1, is an average result from Monte Carlo simulation of EMD on white Gaussian noise. Kopsinis and McLaughlin (2008b, 2009) first investigate iterative EMD denoising and discover that the averaging of different noisy versions by altering the IMF1 of the input signal can increase the S/N of the final output. Although this approach improves the original EMD denoising, it assumes only IMF1 of the input signal is noisy (low S/N case). They further propose the *clear iterative EMD denoising technique* to handle the high S/N case. Our proposed EEMD denoising method is effective for high- and low-S/N cases. We create the noisy versions of the target signal by adding the IMF1 of white noise. Based on the dyadic filter structure of EMD (Flandrin et al., 2004b), the IMF1 of white Gaussian noise contains information in the bandwidth from half-Nyquist to Nyquist frequency, and the added noise can be easily removed using a final band-pass filter.

There are three main parameters in the EEMD thresholding namely, $m1$, $m2$, and σ. Based on the dyadic filter property of each IMF, $m1$ and $m2$ determine approximately the frequency range for thresholding, and the IMFs outside of this range are either removed or untouched. Figure 18 indicates the influence of the thresholding parameter σ on the reference line based on equation 3. It is related to the noise level in the processing and controls the slope of the reference line for denoising. The red, black, and blue solid lines (Figure 18) correspond to $\sigma = 1.2$, 1 and 0.8, respectively. The severity

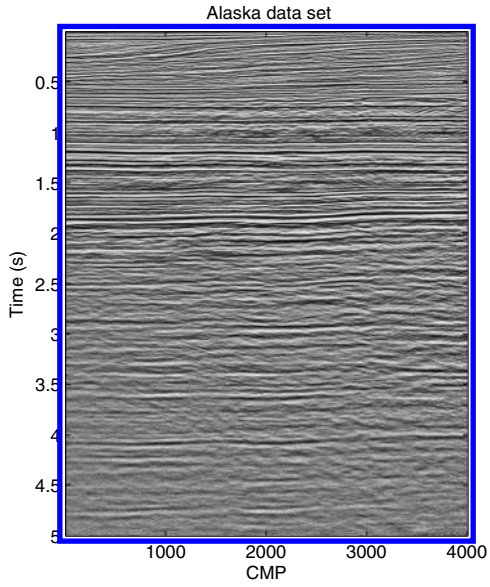

Figure 12. Alaska data. There are the random and coherent noise in the data.

of denoising is proportional to the value of σ. Although the above is the mathematic principle for selecting the parameters, we strongly recommend tests to determine their optimum values for microseismic and seismic processing. Like *f-x* EMD, the proposed *f-x* EEMD denoising is applied in each predefined time window. The window length should balance the performance and computing efficiency; besides, the overlap of the adjacent windows also mitigates the side effects.

Treating the random noise from an inversion view became popular during the last decade in seismic processing (Kumar et al., 2011; Yuan et al., 2012). Hence, basis pursuit obtains similar satisfactory results in the synthetic and microseismic examples. However, it is

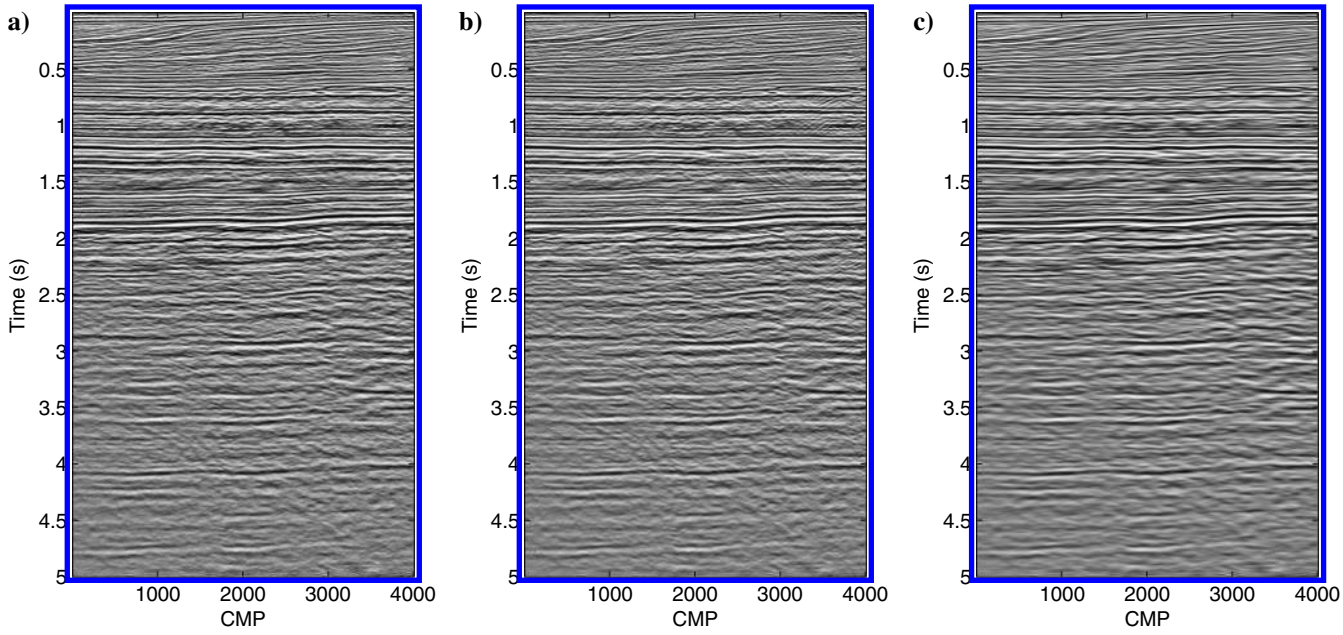

Figure 13. (a) Results of *f-x* EMD. (b) Results of *f-x* deconvolution. (c) Results of *f-x* EEMD thresholding. All three techniques enhance the quality of the original data, especially in the deep part.

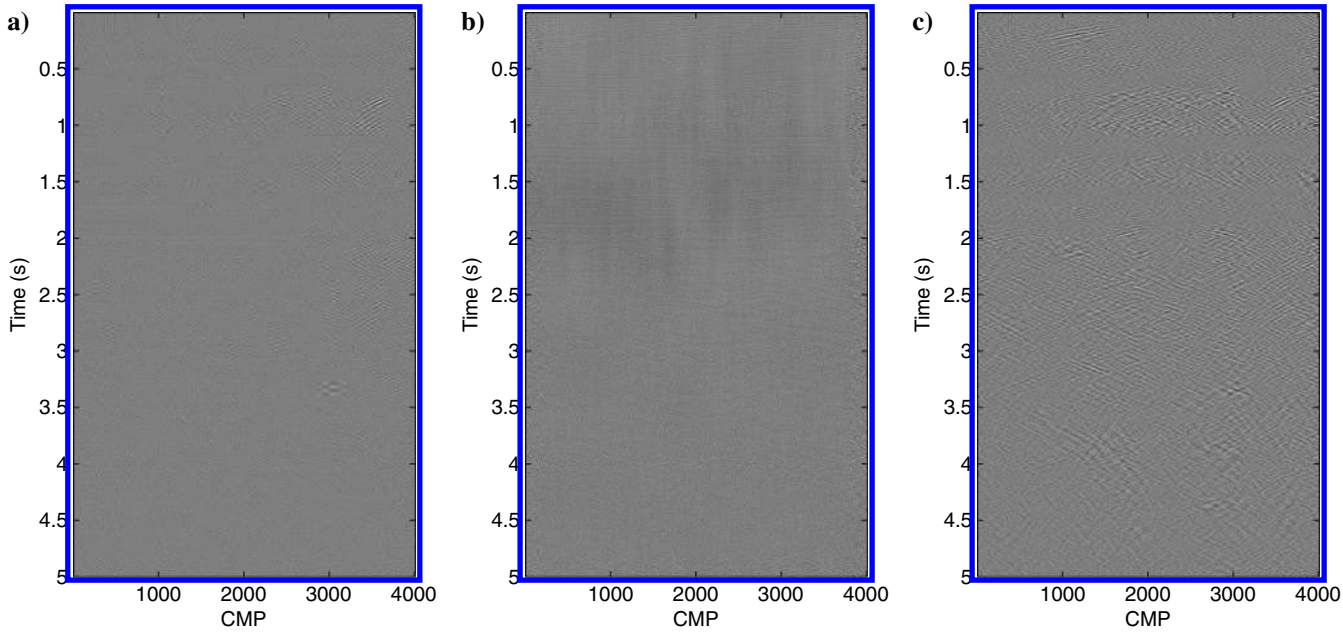

Figure 14. (a) Difference section of *f-x* EMD. (b) Difference section of *f-x* deconvolution. (c) Difference section of the *f-x* EEMD thresholding. No reflections are lost in these methods. The *f-x* deconvolution and *f-x* EEMD thresholding eliminate more noise than does *f-x* EMD.

strongly dependent on the predefined wavelet dictionary. We use the Ricker wavelets as the predefined dictionary in both examples (Vera Rodriguez et al., 2012; Bonar and Sacchi, 2013). The excellent manifestation in the synthetic example is because the predefined dictionary matches the synthetic data exactly, so it only needs a small wavelet dictionary to process. In the microseismic example, the basis pursuit requires a large Ricker wavelet dictionary to match the test events; therefore, it is approximately 15 to 20 times slower than the EEMD thresholding.

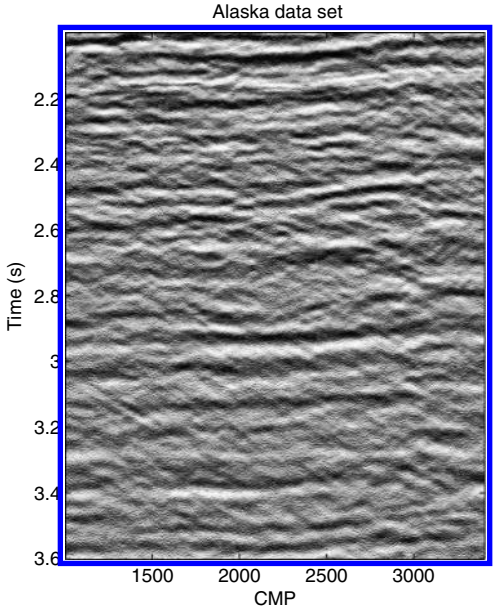

Figure 15. Enlarged section of the Alaska data.

The *f-x* EEMD thresholding manifests its effectiveness in the Alaska data. It combines the advantages of *f-x* deconvolution and *f-x* EMD. The predominance of the AR model in the *f-x* domain is acceptable because of its excellent noise reduction and time-efficient characteristics. However, the theory needs regular trace spacing, and the results of *f-x* deconvolution can enhance any coherent noise as well, such as multiples and dipping energy. Trying EMD as an alternative operator in the *f-x* domain, Bekara and Van der Baan (2009) elaborately discuss the advantages of *f-x* EMD in different kinds of data sets over *f-x* deconvolution. They conclude that *f-x* EMD acts as an autoadaptive wavenumber filter to remove the random and steeply dipping coherence noise. The theory of proposed *f-x* EEMD thresholding is similar as *f-x* EMD. Furthermore, it improves the performance of *f-x* EMD by more parameter controls. The parameter σ is related to the noise level in the seismic data. Random noise pollutes the whole *t-x* domain as well as the *f-x* domain; therefore, thresholding on each IMF in each constant frequency slice is more effective for suppressing random noise than only deleting IMF1. The parameters $m1$ and $m2$ give a flexible control for the dip filter range. Chen and Ma (2014) also talk over the EMD-based dip filter in synthetic seismic data. The Alaska data illustrate that the dipping coherent noise is not totally limited in the IMF1 of each frequency in the *f-x* domain. The proposed *f-x* EEMD thresholding is more powerful in reducing the dipping coherent noise; therefore, it enhances the lateral coherence of the seismic data.

Torres et al. (2011) propose CEEMD, which is a complete version of EEMD. Han and Van der Baan (2013) combine CEEMD with instantaneous spectra for seismic time-frequency analysis, and they conclude that CEEMD solves not only the mode mixing problem, but it also leads to complete signal reconstructions. Therefore, by raising the question, "Why not use the CEEMD thresholding instead of EEMD thresholding?" The answer would be that the

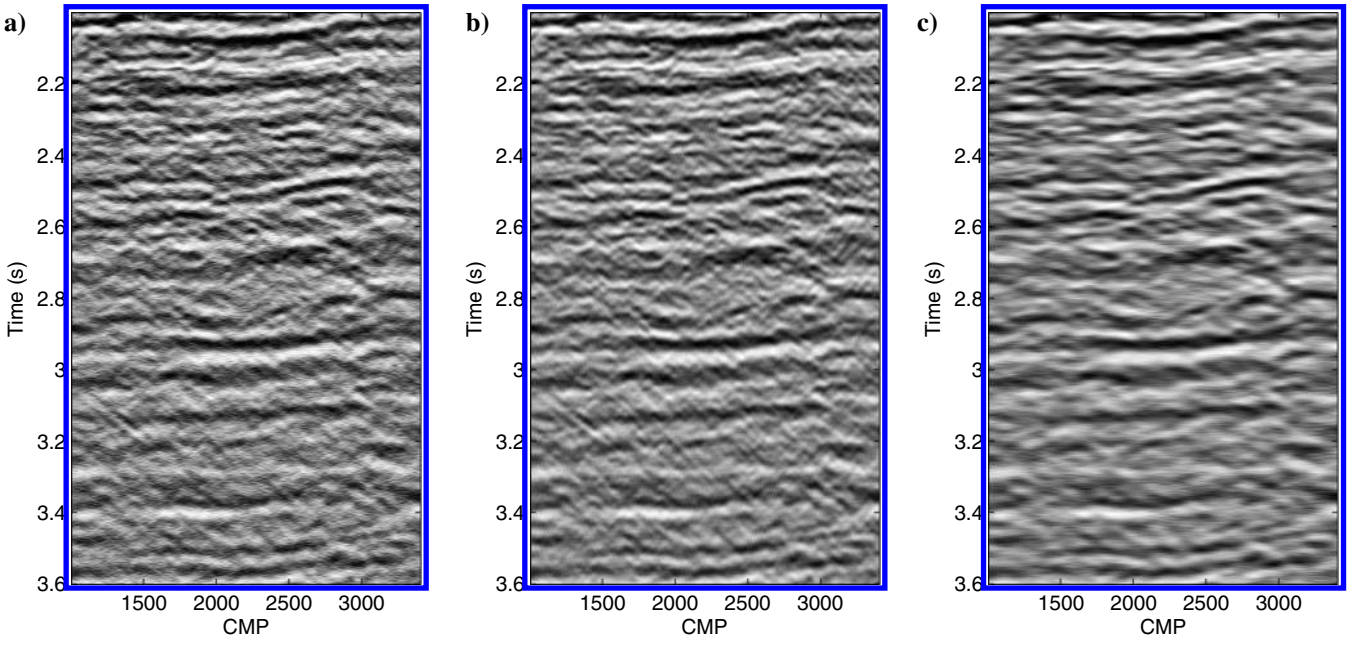

Figure 16. Enlarged section. (a) Result of *f-x* EMD. (b) Result of *f-x* deconvolution. (c) Result of the proposed method. The proposed method obtains the most satisfactory output because the events become clearer than the *f-x* EMD and *f-x* deconvolution.

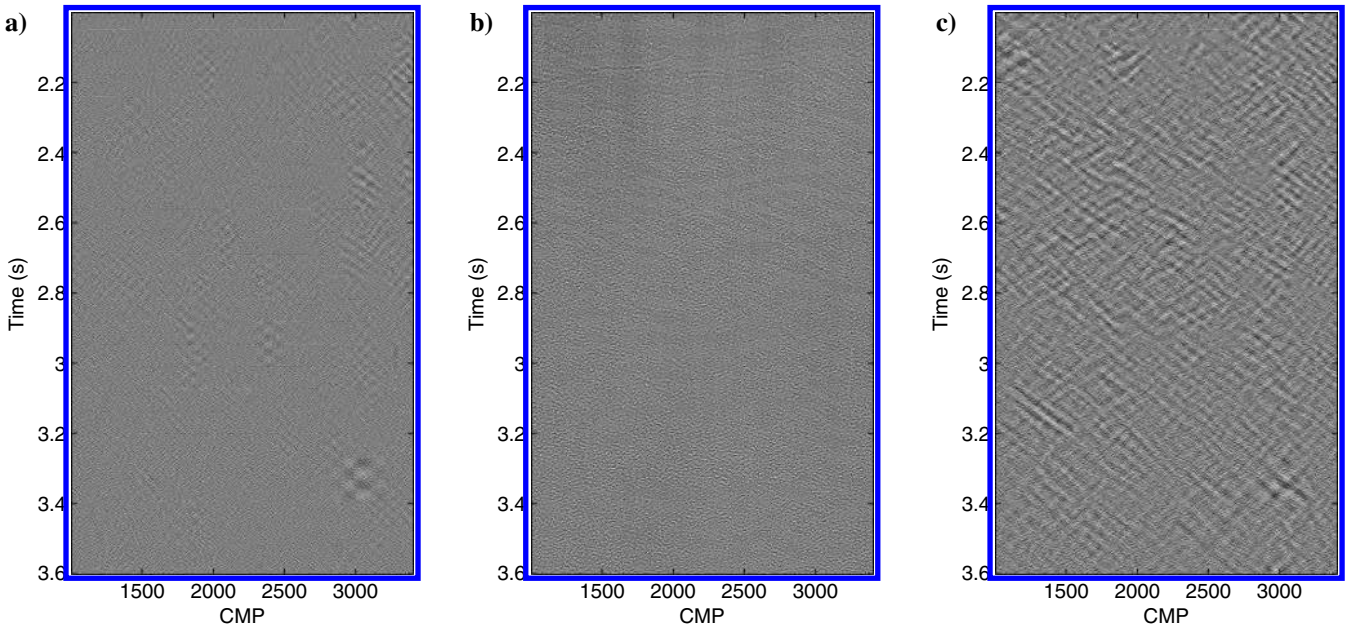

Figure 17. Enlarged section. (a) Difference section of *f-x* EMD. (b) Difference section of *f-x* deconvolution. (c) Difference section of the proposed method. The *f-x* EMD suppresses partial random and coherence noise. The *f-x* deconvolution reduces most random noise without any dipping events. The proposed method eliminates the random noise as well as the coherence noise, such as the dipping noise.

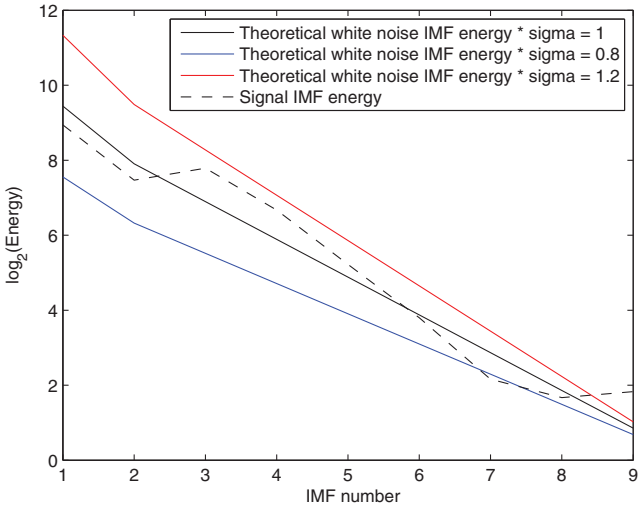

Figure 18. The influence of the thresholding parameter σ on the reference line for denoising. The severity of denoising is proportional to the value of σ.

EMD denoising foundation is based on equation 1, which needs the decomposition of the input signal by the full EMD scheme. In this case, CEEMD does not obey this feature, it uses different decomposition process to obtain each IMF, which simply means that the IMFs energy after CEEMD may not follow equation 1.

CONCLUSIONS

EEMD thresholding is a useful tool for suppressing random noise in the signals with a different S/N because it distinguishes between the structured signal and random noise within each IMF. It can serve as an alternative to simple band-pass filtering with the advantage that it acts as a nonstationary (time-varying), autoadaptive, frequency filter. In this sense, it performs equally well or possibly even better than basis pursuit denoising. If applied in the *f-x* domain, the method acts as a sophisticated wavenumber filter, removing random and dipping coherent noise. It has similar advantages to *f-x* EMD in that it is less sensitive to irregularly spaced data than *f-x* deconvolution; yet this permits for more parameter control as well as an explicit thresholding scheme designed to remove random noise. The synthetic, microseismic, and reflection seismic examples illustrate the good performance of the proposed methods.

ACKNOWLEDGMENTS

The authors thank Chevron and Statoil for the financial support of the project Blind Identification of Seismic Signals (BLISS), L. Han for providing the synthetic data, M. Sacchi for sharing the basis pursuit code, an anonymous company for permission to show the microseismic event, and the United States Geological Survey for use of the Alaska data set. We are also grateful to S. Yuan, Y. Chen, and J. I. Sabbione for their many comments and suggestions.

REFERENCES

Battista, B., C. Knapp, T. McGee, and V. Goebel, 2007, Application of the empirical mode decomposition and Hilbert-Huang transform to seismic reflection data: Geophysics, **72**, no. 2, H29–H37, doi: 10.1190/1.2437700.

Bekara, M., and M. Van der Baan, 2009, Random and coherent noise attenuation by empirical mode decomposition: Geophysics, **74**, no. 5, V89–V98, doi: 10.1190/1.3157244.

Bonar, D., and M. Sacchi, 2013, Spectral decomposition with *f-x-y* preconditioning: Geophysical Prospecting, **61**, 152–165, doi: 10.1111/j.1365-2478.2012.01104.x.

Boudraa, A., and J. Cexus, 2006, Denoising via empirical mode decomposition: Presented at IEEE International Symposium on Communications, Control and Signal Processing.

Canales, L., 1984, Random noise reduction: 54th Annual International Meeting, SEG, Expanded Abstracts, 525–527.
Castellanos, F., and M. van der Baan, 2013, Microseismic event locations using the double-difference algorithm: CSEG Recorder, **38**, 26–37.
Chen, S., D. Donoho, and M. Saunders, 2001, Atomic decomposition by basis pursuit: SIAM Journal on Scientific Computing, **43**, 129–159, doi: 10.1137/S003614450037906X.
Chen, Y., and J. Ma, 2014, Random noise attenuation by *fx* empirical-mode decomposition predictive filtering: Geophysics, **79**, no. 3, V81–V91, doi: 10.1190/geo2013-0080.1.
Dong, L., Z. Li, and D. Wang, 2013, Curvelet threshold denoising joint with empirical mode decomposition: 83rd Annual International Meeting, SEG, Expanded Abstracts, 4412–4416.
Donoho, D., 1995, De-noising by soft-thresholding: IEEE Transactions on Information Theory, **41**, 613–627, doi: 10.1109/18.382009.
Donoho, D., and J. Johnstone, 1994, Ideal spatial adaptation by wavelet shrinkage: Biometrika, **81**, 425–455, doi: 10.1093/biomet/81.3.425.
Flandrin, P., P. Goncalves, and G. Rilling, 2004a, Detrending and denoising with empirical mode decompositions: Presented at European Signal Processing Conference, Citeseer, 1581–1584.
Flandrin, P., G. Rilling, and P. Goncalves, 2004b, Empirical mode decomposition as a filter bank: IEEE Signal Processing Letters, **11**, 112–114, doi: 10.1109/LSP.2003.821662.
Geological Survey, U.S., 1981, http://wiki.seg.org/wiki/ALASKA_2D_LAND_LINE_31-81, accessed 2 January 2015.
Han, J., and M. Van der Baan, 2011, Empirical mode decomposition and robust seismic attribute analysis: Presented at 2011 CSPG CSEG CWLS Convention.
Han, J., and M. Van der Baan, 2013, Empirical mode decomposition for seismic time-frequency analysis: Geophysics, **78**, no. 2, O9–O19, doi: 10.1190/geo2012-0199.1.
Han, L., M. Sacchi, and L. Han, 2014, Spectral decomposition and de-noising via time- frequency and space-wavenumber reassignment: Geophysical Prospecting, **62**, 244–257, doi: 10.1111/1365-2478.12088.
Herrera, R., J. Han, and M. Van der Baan, 2014, Applications of the synchrosqueezing transform in seismic time-frequency analysis: Geophysics, **79**, no. 3, V55–V64, doi: 10.1190/geo2013-0204.1.
Huang, N., and Z. Wu, 2008, A review on Hilbert-Huang transform: Method and its applications to geophysical studies: Reviews of Geophysics, **46**, RG2006, doi: 10.1029/2007RG000228.
Huang, N. E., Z. Shen, S. R. Long, M. C. Wu, H. H. Shih, Q. Zheng, N.-C. Yen, C. C. Tung, and H. H. Liu, 1998, The empirical mode decomposition and the Hilbert spectrum for nonlinear and non-stationary time series analysis: Proceedings A — The Royal Society, doi: 10.1098/rspa.1998.0193.
Kopsinis, Y., and S. McLaughlin, 2008a, Empirical mode decomposition based denoising techniques: 1st IAPR Workshop on Cognitive Information, 42–47.
Kopsinis, Y., and S. McLaughlin, 2008b, Empirical mode decomposition based soft-thresholding: Presented at 16th European Signal Processing Conference — EUSIPCO, 1–5.
Kopsinis, Y., and S. McLaughlin, 2009, Development of EMD-based denoising methods inspired by wavelet thresholding: IEEE Transactions on Signal Processing, **57**, 1351–1362, doi: 10.1109/TSP.2009.2013885.
Kumar, V., J. Oueity, R. Clowes, and F. Herrmann, 2011, Enhancing crustal reflection data through curvelet denoising: Tectonophysics, **508**, 106–116, doi: 10.1016/j.tecto.2010.07.017.
Magrin-Chagnolleau, I., and R. Baraniuk, 1999, Empirical mode decomposition based time-frequency attributes: 69th Annual International Meeting, SEG, Expanded Abstracts, 1949–1952.
Mandic, D., Z. Wu, and N. E. H., 2013, Empirical mode decomposition-based time- frequency analysis of multivariate signals: The power of adaptive data analysis: IEEE Signal Processing Magazine, **30**, no. 6, 74–86, doi: 10.1109/MSP.2013.2267931.
Sacchi, M., and H. Kuehl, 2001, ARMA formulation of FX prediction error filters and projection filters: Journal of Seismic Exploration, **9**, 185–197.
Song, H., Y. Bai, L. Pinheiro, C. Dong, X. Huang, and B. Liu, 2012, Analysis of ocean internal waves imaged by multichannel reflection seismics, using ensemble empirical mode decomposition: Journal of Geophysics and Engineering, **9**, 302–311, doi: 10.1088/1742-2132/9/3/302.
Soubaras, R., 1994, Signal-preserving random noise attenuation by the *f-x* projection: 64th Annual International Meeting, SEG, Expanded Abstracts, 1576–1579.
Tary, J.-B., R. Herrera, J. Han, and M. Van der baan, 2014, Spectral estimation — What is new? What is next?: Reviews of Geophysics, **52**, 723–749, doi: 10.1002/2014RG000461.
Tong, W., M. Zhang, Q. Yu, and H. Zhang, 2012, Comparing the applications of EMD and EEMD on time-frequency analysis of seismic signal: Journal of Applied Geophysics, **83**, 29–34, doi: 10.1016/j.jappgeo.2012.05.002.
Torres, M., M. Colominas, G. Schlotthauer, and P. Flandrin, 2011, A complete ensemble empirical mode decomposition with adaptive noise: Presented at 2011 IEEE International Conference on Acoustics, Speech and Signal Processing, 4144–4147.
Tsolis, G., and T. Xenos, 2011, Signal denoising using empirical mode decomposition and higher order statistics: International Journal of Signal Processing, Image Processing and Pattern Recognition, **4**, 91–106.
Vera Rodriguez, I., D. Bonar, and M. Sacchi, 2012, Microseismic data denoising using a 3C group sparsity constrained time-frequency transform: Geophysics, **77**, no. 2, V21–V29, doi: 10.1190/geo2011-0260.1.
Wu, Z., and N. E. Huang, 2004, A study of the characteristics of white noise using the empirical mode decomposition method: Proceedings of the Royal Society A: Mathematical, Physical and Engineering Sciences, **460**, 1597–1611, doi: 10.1098/rspa.2003.1221.
Wu, Z., and N. E. Huang, 2009, Ensemble empirical mode decomposition: A noise-assisted data analysis method: Advances in Adaptive Data Analysis, **01**, 1–41, doi: 10.1142/S1793536909000047.
Xue, Y., J. Cao, and R. Tian, 2014, EMD and Teager-Kaiser energy applied to hydrocarbon detection in a carbonate reservoir: Geophysical Journal International, **197**, 277–291, doi: 10.1093/gji/ggt530.
Yuan, S., S. Wang, and G. Li, 2012, Random noise reduction using Bayesian inversion: Journal of Geophysics and Engineering, **9**, 60–68, doi: 10.1088/1742-2132/9/1/007.